Ultra-Efficient Electrolytic Ocean Carbon Removal Through Capacitive Decarbon Reactors

Yifang Zhu[1], Yang Ou[2,3], Jay Fuhrman[4], Meng Lin[5], Kuichang Zuo[1*], Huazhang Zhao[1*], Zishuai Bill Zhang[1,3*]

[1]The Key Laboratory of Water and Sediment Sciences, Ministry of Education, College of Environmental Sciences and Engineering, Peking University, Beijing, 100871, China

[2]College of Environmental Sciences and Engineering, Peking University, Beijing, 100871, China

[3]Institute of Carbon Neutrality, Peking University, Beijing 100871, China

[4]Joint Global Change Research Institute, University of Maryland and Pacific Northwest National Laboratory, College Park, MD, USA

[5]SUSTech Energy Institute for Carbon Neutrality, Department of Mechanical and Energy Engineering, Southern University of Science and Technology, Shenzhen 518055, China

*Correspondence: Kuichang Zuo (kuichang.zuo@pku.edu.cn)

Huazhang Zhao (zhaohuazhang@pku.edu.cn)

Zishuai Bill Zhang (zszhang@pku.edu.cn)

Abstract

Direct ocean capture (DOC) is a promising technique for mitigating residual anthropogenic CO_2 levels. However, the existing DOC methods are energy-intensive and may have unforeseen effects on marine ecosystems due to the chemical processes involved. We introduce a capacitive decarbon (CDC) reactor that converts carbonate ions into $CaCO_3$, a construction material, using only calcium ions (Ca^{2+}) from seawater and renewable electricity. After optimizations of the electrode and electrolytic reactor, the CDC reactor achieves ocean carbon removal with an exceptionally low energy consumption of 16 kJ mol^{-1} CO_2, which is one order of magnitude lower than previously reported values. This energy requirement increases to 107 kJ mol^{-1} CO_2 when factoring in the seawater intake and pre-treatment. We then used a global integrated analysis model to evaluate the carbon mitigation potential of this approach and found that it can remove about 360 to 1,670 million tonnes of CO_2 in 2050 and 2100, respectively, which corresponds to 4.55% and 14.82% of the global carbon sequestration capacity for those years. Given the high efficiency of the CDC reactor, we anticipate it may become a viable solution for sequestering oceanic carbon.

The reduction of residual anthropogenic carbon dioxide (CO_2) concentrations necessitates the direct CO_2 removal from the atmosphere and oceans(*1*). One of the typical processes, known as the direct air capture (DAC), employs advanced (electro)chemical processes to capture CO_2 from atmosphere, followed by CO_2 liberation through temperature, pressure or pH swings (Fig. 1a)(*2*–*5*). The liberated CO_2 then undergoes purification and pressurization before being transported for utilization or storage (Fig. 1a)(*2*, *3*). Due to the exceedingly low concentration of CO_2 in the atmosphere (~410 ppm), and the intricate multistep nature of process, the energy consumption of the current DAC technologies is prohibitively high (200 – 365 kJ mol^{-1} CO_2) for gigatonne scale implementation(*6*). Moreover, the substantial capital and maintenance costs (currently over \$100 t^{-1} CO_2) associated with DAC systems present monumental challenges to scale up these techniques(*7*).

A promising alternative for DAC is the direct ocean capture (DOC). This is largely because the ocean serves as the largest carbon sink (~139,000 Gt), with an effective CO_2 concentration (in the forms of CO_3^{2-} or HCO_3^-) of 2.1 – 2.2 mmol kg^{-1}, which is over 100 times greater than that in the atmosphere(*8*, *9*). To date, several representative strategies have been proposed to capture oceanic CO_2 including the electrochemical pH swing(*8*, *10*) and the thermal calcium (Ca) looping(*11*, *12*). In the electrochemical pH swing approach, seawater is split into acid and base electrochemically. The acid is utilized to acidify seawater, prompting the conversion of CO_3^{2-} or HCO_3^- to dissolved CO_2 that is subsequently extracted using a membrane contactor(*8*). The base is then used to neutralize the acidified seawater, and the resulting neutralized seawater is discharged back into the ocean(*8*). The thermal Ca looping involves the calcination of minerals such as limestone ($CaCO_3$), a process which yields CaO and also release CO_2 (Eq. 1). CaO is then introduced into seawater as the concentrated Ca^{2+} source and raises the seawater pH, thereby

facilitating the formation of $CaCO_3$, effectively closing the loop. Both approaches require substantial energy inputs due to the high-energy reactions involved (such as water dissociation and carbonate calcination), with the most efficient DOC technology exhibiting the energy consumption ranging from 120 to 200 kJ mol^{-1} CO_2(*8*, *10*). Considering the additional energies required for seawater intake and pre-treatment, it is highly probable that the total energy penalty will exceed 500 kJ mol^{-1} CO_2 in practice(*8*). Furthermore, chemical reactions, such as the Cl^- oxidation in the electrochemical pH swing method, could have implications for the safety of marine ecosystems(*10*).

The carbon capture process must be coupled with downstream CO_2 conversion or storage to effectively achieve meaningful carbon removal(*13*–*15*). One such strategy involves converting CO_2 into small molecules including carbon monoxide (CO)(*13*–*16*), ethylene (C_2H_4)(*17*), and alcohols (CH_3OH, C_2H_6O)(*18*), enabling the production of carbon−neutral chemicals and fuels (Fig. 1a). However, this method only provides temporary CO_2 storage lasting from months to years (Fig. 1a)(*19*). Furthermore, the energy consumption associated with CO_2 conversion typically ranges from 600 to 800 kJ mol^{-1} CO_2(*19*), resulting in a total energy expenditure of 720 to 1165 kJ mol^{-1} CO_2 for the ocean carbon capture−utilization scheme (Fig. 1b). Captured CO_2 can alternatively mineralize with natural silicates, which offers a permanent solution rather than short−term storage(*20*). However, the kinetics of mineralization are generally sluggish and cannot meet the CO_2 capture rates(*21*). Fast mineralization needs the pre−treatment of the silicates that requires grinding energy inputs of 25 to 130 kJ mol^{-1} CO_2(*22*). Additionally, the current carbon capture – utilization facilities require intensive land and water usages(*11*, *12*). These concerns collectively motivate us to develop an energy efficient, resource (e.g., land and water) independent and chemical−free technology for permanent ocean carbon removal.

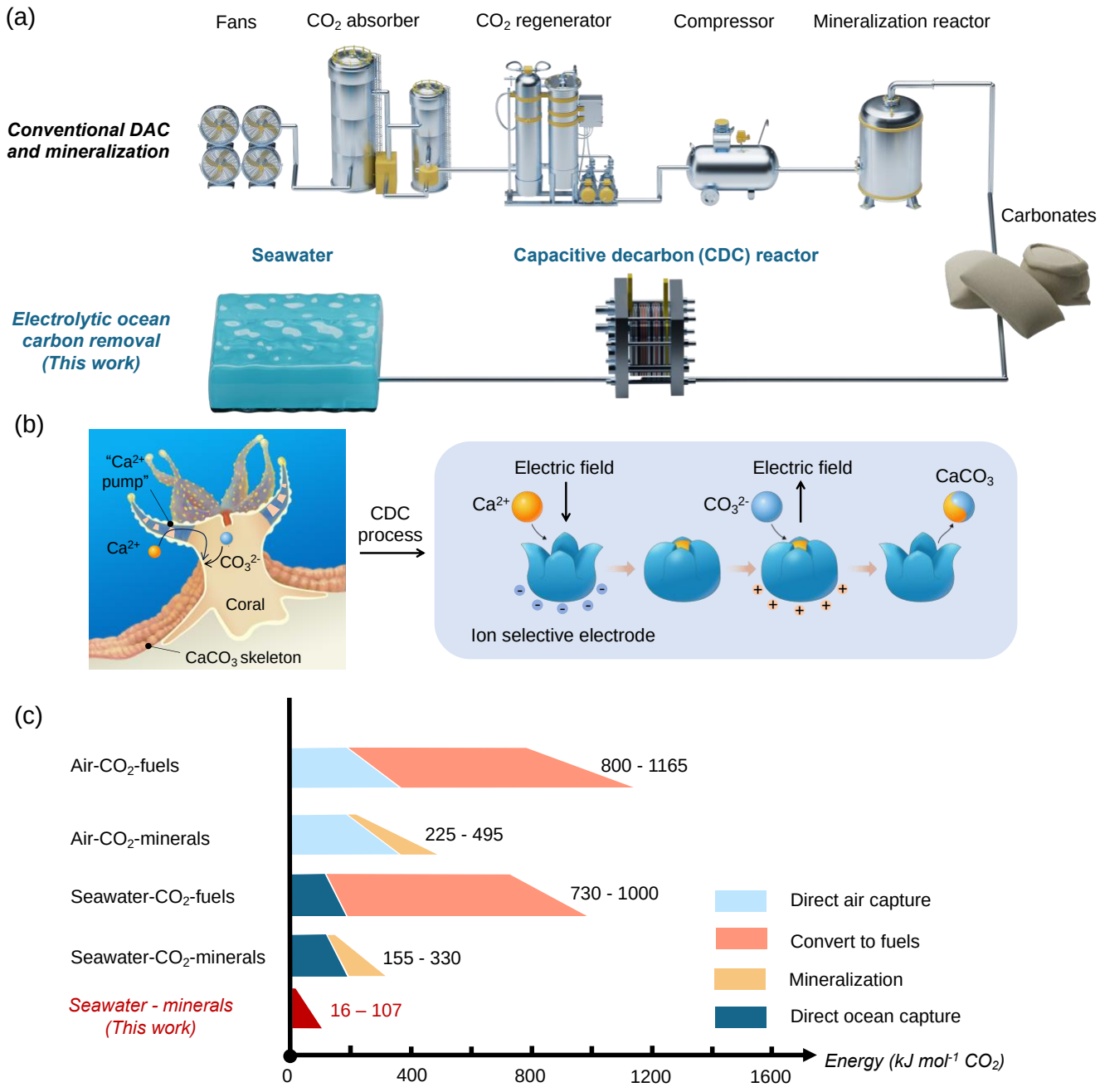

Fig. 1. Conventional carbon capture and utilization process and the CDC process for carbon removal. (a) Process flow diagram of conventional DAC and mineralization scheme and direct ocean carbon removal scheme (this work). The left corner is the schematic illustration of the CDC process for $CaCO_3$ formation (the figure of ion selective electrode is adopted from the enzyme demonstration of the ACS Science Outreach), and the right corner is the energy landscapes from carbon to CO_2 conversion products. (d) Energy analysis of diverse CO_2 removal techniques from air and seawater. In the trapezoidal

illustration, the shorter base corresponds to the minimum level of energy usage, while the longer base denotes the maximum level of energy consumptions.

Inspired by the corals' ability to selectively capture Ca^{2+} ions from seawater through "Ca^{2+} pumps" and combine them with CO_3^{2-} ions to form their $CaCO_3$ skeletons(*23*), we have designed an electrolytic reactor (i.e., CDC reactor) that can emulate this natural calcification process, effectively sequestrating ocean carbon as $CaCO_3$ using only CO_3^{2-} and Ca^{2+} ions from seawater. The operating principle of the CDC reactor is similar to a capacitive deionization (CDI) system, which is engineered to manage the migration of ions through electric fields(*24*). A notable feature of a CDC reactor is an efficient ion-selective electrode that can selectively bind with Ca^{2+}, resulting in a concentrated region of Ca^{2+} ions at the electrode's surface (Fig. 1a). Subsequently, the potential polarization is reversed to attract CO_3^{2-} ions, which creates a region with high concentrations of CO_3^{2-} and Ca^{2+} ions, promoting the formation of $CaCO_3$ (Fig. 1a).

Initially, we focused on improving the performance of the ion-selective electrode by refining its composition and morphology, optimizing the functional groups and maximizing the exposure density of these functional groups. Following this improvement, we conducted a reactor-level optimization by fine-tuning parameters such as the electrode distance, feedstock flowrate, and applied voltages to achieve the highest carbon removal efficiency. These efforts resulted in an exceptionally low energy consumption of 16 kJ mol^{-1} CO_2 for the CDC process, which is one order of magnitude lower than previously reported values (Fig. 1b). To comprehensively assess the potential impact of the CDC technique on global carbon mitigation efforts, we utilized the Global Change Analysis Model (GCAM). This integrated assessment model offers a full understanding of the complex interplay between climate change and global energy systems. With the scenario in which CO_2

emissions are constrained to limit warming to below 1.5 °C in 2100, we have evaluated the potential global impact of this approach and found it can remove 357 to 1,666 million tonnes of CO_2 in 2050 and 2100, respectively, equating to 4.55% and 14.82% of the global carbon sequestration capacity for those years, with America and China leading this change, potentially eliminating 109 and 68 million tonnes of CO_2 respectively in 2050.

Ca^{2+} selective electrodes enable Ca^{2+} ion enrichment from seawater

A major challenge in DOC techniques is to capture the ultra-diluted CO_3^{2-} or HCO_3^- (the forms of CO_2 in seawater) in seawater. One established method involves introducing Ca^{2+} ions into seawater to precipitate with CO_3^{2-}(*8*). However, the production of active Ca^{2+} containing chemicals (such as CaO) is energetically costly (Fig. 2a)(*22*). Given the fact that the amount of Ca^{2+} (~10 mM) in seawater is sufficient to mineralize all CO_3^{2-} or HCO_3^- present (in total ~2-3 mM), it is reasonable to consider utilizing the abundant Ca^{2+} in seawater to remove CO_3^{2-}, rather than introduce it from an external source.

The key step in this approach is to concentrate Ca^{2+} in a localized region to a level that enables $CaCO_3$ formation. We therefore developed a Ca^{2+} selective electrode for this purpose. The active component of the Ca^{2+} selective electrode is the polymers with functional groups that can selectively bind with Ca^{2+}. However, the binding affinity between the selected functional groups and Ca^{2+} must be carefully chosen. An excessively strong binding energy (e.g., $-COO^-$, $-PO_3^{2-}$, $-PO_4^{2-}$) would prevent the bounded Ca^{2+} to react with CO_3^{2-} (no precipitation was observed), while a weak binding energy (e.g., $-SO_4^-$, $-OH$) would result in ineffective capture of Ca^{2+} (Fig. 2b). We therefore selected $-SO_3^-$ due to its optimal binding affinity with Ca^{2+} (Fig. 2b).

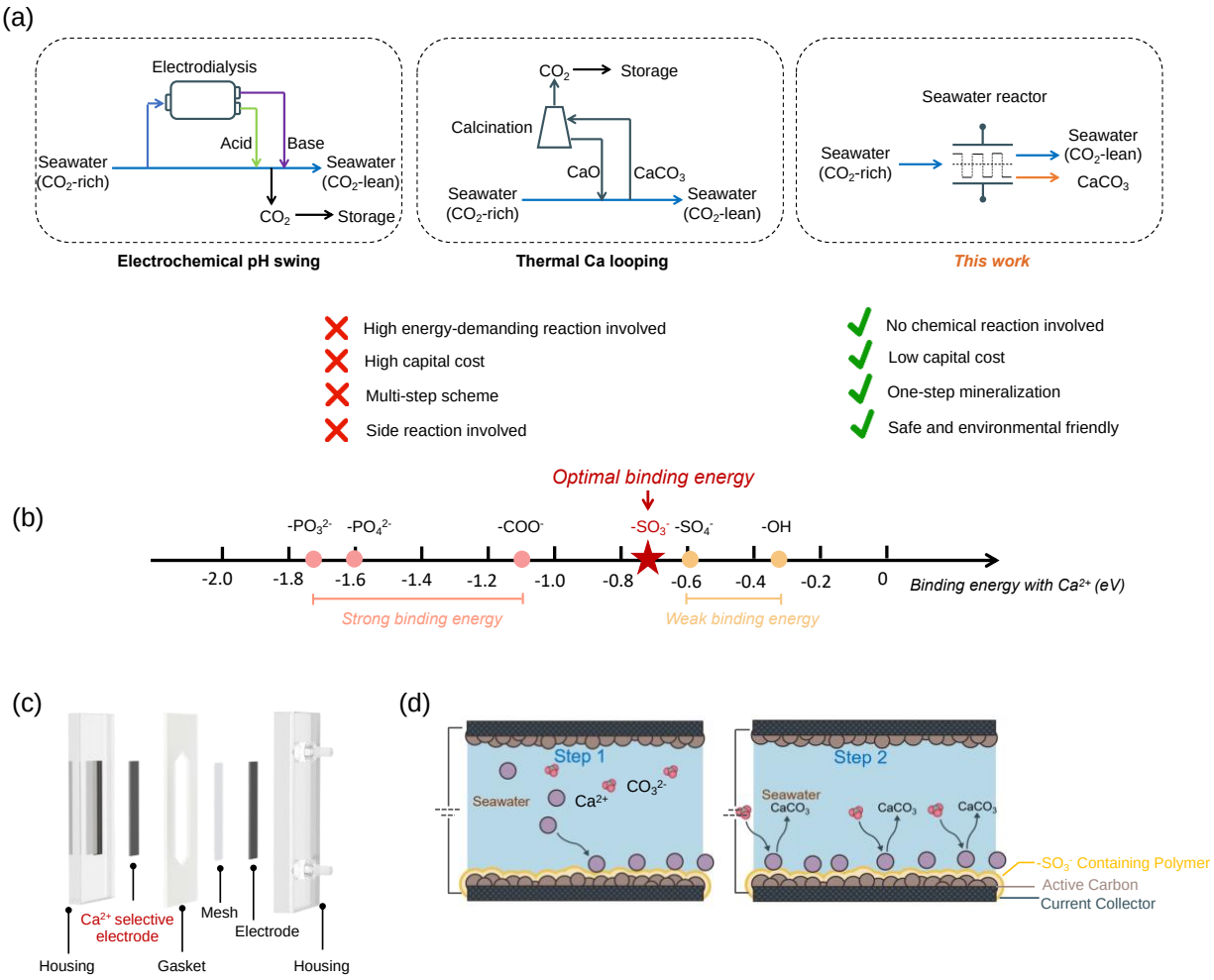

Fig. 2. Capacitive decarbon (CDC) design. (a) A comparative illustration of techniques for the carbon removal from seawater. The electrochemical pH swing and thermal Ca looping techniques rely on energetically intensive reactions. Conversely, the CDC process offers a single-step mechanism for the mineralization of CO_2 into $CaCO_3$, facilitating the long-term sequestration of CO_2. (b) Comparison of the binding energies of Ca^{2+} ions with various anions ($-PO_3^{2-}$, $-PO_4^{2-}$, $-COO^-$, $-SO_3^-$,$-SO_4^-$, -OH), suggesting that $-SO_3^-$ possesses the optimal binding energy for the CDC method. (c) Schematic illustration of the CDC reactor, the capture of Ca^{2+} ions and the subsequent formation of $CaCO_3$ primarily rely on a Ca^{2+}-selective electrode. (d) The experimental operating principle for the CDC technique. The $CaCO_3$ formation is achieved by alternating the the applied potentail between electrodes.

We first tested the Ca^{2+} selectivity of the electrode in a custom−designed CDC reactor (Fig. 2c; See Supplementary Note 1). Homogeneous ink, consisting of active carbon (AC) powder with polymeric binders (poly(vinyl alcohol) and glutaraldehyde), was flow coated on a graphite

sheet (that measured 1 cm by 5 cm) (Figs. S2-S5). The resulting electrode was dried and annealed prior to use (denoted as "**AC electrode**"). A Nafion layer (Fig. S6), which contains 0.9 mmol $-SO_3^-$ functional group per gram (ion exchange capacity of 0.9 mmol g^{-1}), was spray coated on the **AC electrode** to fabricate the Ca^{2+} selective electrode (denoted as "**Nafion electrode**"). Both the **AC electrode** and **Nafion electrode** contain same quantity of AC. A plastic mesh was employed to separate anode and cathode and facilitate homogeneous flow distribution. Gaskets, with thickness ranging from 1 to 2 mm, were inserted between the anode and cathode to prevent leakage and control distances between electrodes. The seawater feedstock was continuously recirculating into the CDC reactor at a flow rate ranging from 1.5 to 4.5 mL min^{-1}, and the applied voltage between electrodes are set ranging from 0 to 1.2 V to prevent water splitting.

The selectivity of $-SO_3^-$ functional group towards Ca^{2+} (and Mg^{2+}) ions were tested using the **AC electrode** and **Nafion electrode** under a voltage cycling experiment (Figs. 3, S7). In each voltage cycle, a negative voltage of -1.2 V was applied for 15 mins to bind cations (such as Na^+ and Ca^{2+} ions, followed by cation release at 0 V for 15 mins. Net amount of captured Ca^{2+} and Na^+ on the electrodes can be quantified using the inductively coupled plasma optical emission spectroscopy (ICP-OES). Due to the limited number of ions that can be adsorbed using a 5 cm^2 electrode, we used diluted Ca^{2+} and Na^+ concentrations of approximately 1 mol% of the Ca^{2+} and Na^+ concentrations in seawater, to highlight the cation concentration changes and reduce experiment errors.

Following the two initial cycles, the Ca^{2+} concentration siginificantly decreased from 34.03 to 18.99 mg L^{-1}, and further declined to 8.99 mg L^{-1} (a total 73.6% decrease) after 20 cycles with a **Nafion electrode** (Fig. 3a), with only minimal of Na^+ ions being adsorbed. The current efficiency for binding Ca^{2+} was initially ~100% for the initial cycle, indicating a high binding affinity

between $-SO_3^-$ and Ca^{2+} (Fig. S8). The results also indicated Ca^{2+} would not be released back to the solution without applied voltage. A distinct Ca−O bonding signal was observed in the X−ray photoelectron spectroscopy (XPS) spectrum after voltage cycling (Fig. S9), confirming the Ca^{2+} formed stable covalent bonds with $-SO_3^-$. A bare **AC electrode** also exhibited a relatively high selectivity towards Ca^{2+}, although significantly lower than that with the $-SO_3^-$ coating, which can be attributed to the steric effect (Fig. 3b).

After conducting 10 cycles of testing, we observed that the **Nafion electrode** can no longer adsorb Ca^{2+}. To validate the performance the designed electrode, especially under conditions of low Ca^{2+} concentration, we replaced the **Nafion electrode** and found this strategy can effectively depleted the Ca^{2+} ions (Fig. 3e). This result indicates that the designed electrode can adsorb Ca^{2+} ions at minimal concentrations. We further explored the impact of $-SO_3^-$ loading on the Ca^{2+} adsorption capacity. Increasing a 50 wt% of Nafion loading on a **Nafion electrode** resulted in only a marginal 2 wt% increase in adsorbed Ca^{2+}, suggesting most active Ca^{2+} selective region of the **Nafion electrode** located at its surface, possibly due to its dense layer structure (Fig. S10).

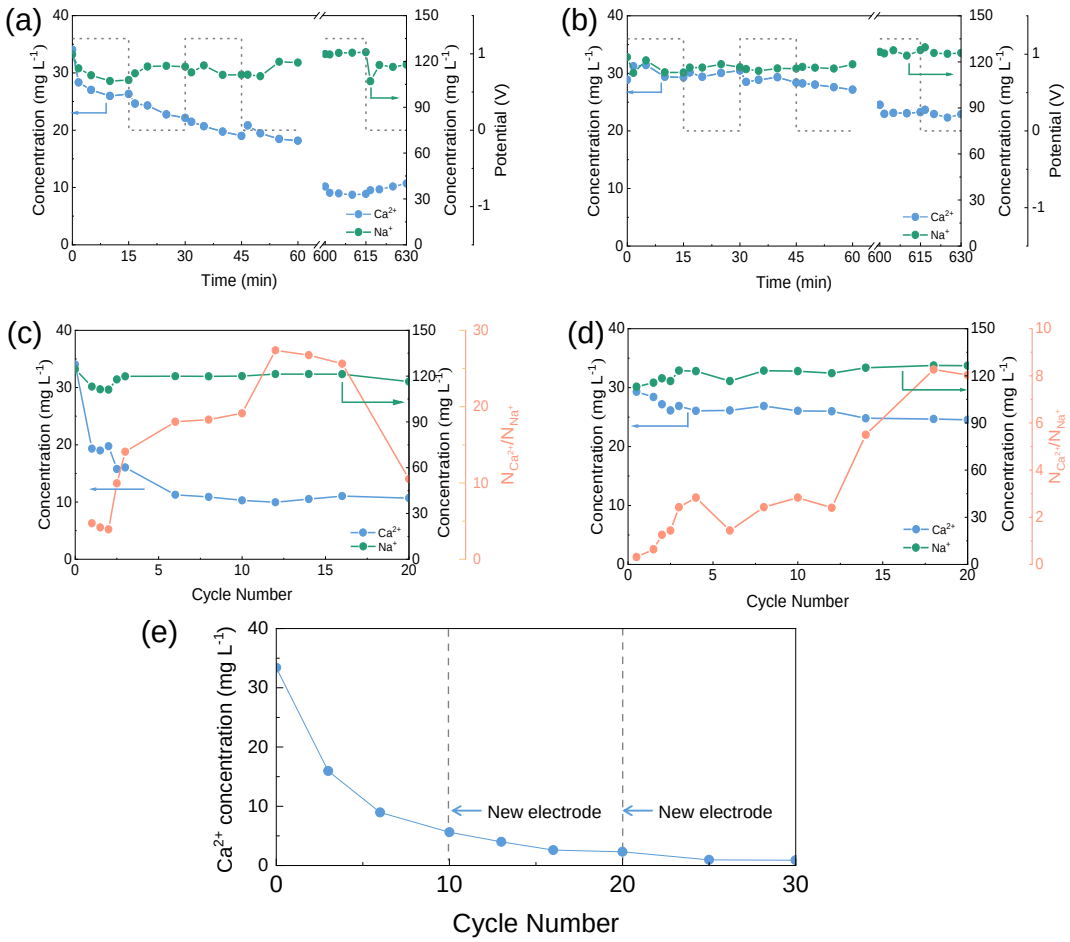

Fig. 3. The selective Ca^{2+} binding on the Nafion electrode. (a) Changes in the cation concentration when using a **Nafion electrode** (a) and a **AC electrode** (b) in a CDC reactor over 600 mins. The light blue lines represent the Ca^{2+} ion concentration, and the green lines represent the change in Na^{+} ions in the solution that contains 1% of Na^{+} and Ca^{2+} ions of the seawater. Coresponding variations in ion concentrations when using a **Nafion electrode** (c) and a **AC electrode** (d) in a CDC reactor cell during different numbers ofcharge and discharge cycles, the orange lines represent the cumulative amount of Ca^{2+} ions relative to Na^{+} ions. (e) The Ca^{2+} concentration change profile with the strategy of replacing the **Nafion electrode**.

CDC reactor for carbon removal

After confirming the high Ca^{2+} selectivity of the **Nafion electrode**, we evaluated the carbon removal performance using a CDC reactor (See Supplementary Note 2). However, we observed no detectable $CaCO_3$ precipitation after voltage cycling (at the potential of $\pm$1.2 V) (Fig. 4a) in

simulated seawater (Tab. S1). We then doubled the Ca^{2+} concentration in the solution, which results in the formation of $CaCO_3$. Consequently, we concluded that a high local Ca^{2+} concentration at the electrode surface is essential for $CaCO_3$ formation, and this could be accomplished by increasing the accessible $-SO_3^-$ density (active sites for binding Ca^{2+}) at the electrode surface. Simply increasing the Nafion loading did not yield the desired results, as the dense layer of Nafion was only active at the surface layer, which was consistent with our previous findings. We therefore employed polystyrene sulfonic (PSS) resins which contains a much higher ion exchange capacity of 5.8 mmol g^{-1} to fabricate an efficient Ca^{2+} selective electrode with high porosity (denoted as "**PSS electrode**") using fine PSS powders (Figs. S4, S11). The experimental results showed increasing the density of accessible $-SO_3^-$ of the electrode leads to $CaCO_3$ formation at the oceanic ion concentration (Fig. 4a).

The energy consumption of ocean carbon removal and conversion rate (CR) of the inorganic carbons (CO_3^{2-} or HCO_3^-) are quantified by measuring the mass of produced $CaCO_3$ in 1 liter (L) of simulated seawaters using the **PSS electrode** (Eqs. 5 and 6). The impact of SO_4^{2-} on the $CaCO_3$ formation has been identified using both full spectrum seawater and simulated seawater without SO_4^{2-} (Fig. 4b). These performances are found to be directly related to the applied voltage, seawater flow rates and electrode distances. The formation of $CaCO_3$ involves two main steps: nucleation and growth. Firstly, voltage cycling experiments were conducted to initiate $CaCO_3$ nucleation, followed by a 20 h rest to allow for the $CaCO_3$ growth.

$$\text{Energy consumption} = \frac{U \int_{t_1}^{t_2} |I(t)| \, dt}{m_{CaCO_3} / M_{CaCO_3}} \qquad \text{Eq. 5}$$

$$\text{Conversion rate (CR)} = \frac{m_{CaCO_3} / M_{CaCO_3}}{c(CO_3^{2-}) + c(HCO_3^-)} \qquad \text{Eq. 6}$$

where, m_{CaCO_3} is the mass of $CaCO_3$ obtained (g), $|I(t)|$ (A) is the cathodic current, U (V) is the applied potential, dt (s) is the operational time.

We determined the optimal seawater flow rate for $CaCO_3$ formation to be between 1.5 and 4.5 ml min^{-1} (Fig. S12), and a shorter electrode distance results in a lower $CaCO_3$ formation energy (Figs. S13-S15). The minimal electrode distance of 1 mm in this study, and we anticipate that further improvements in performance can be achieved by continuing to decrease the electrode distance, however, a thinner flow channel could potentially result in increased flow resistance and an elevated risk of short-circuiting.

The $CaCO_3$ formation was not observed when the applied voltage was below 0.4 V, potentially caused by the insufficient local Ca^{2+} concentration at the electrode surface (Fig. 4b). A higher voltage leads to a greater amount of Ca^{2+} ions stored at the electrode, similar to the capacitor charging process. Therefore, the mass of the $CaCO_3$ and the CR values increases with the increase of the applied voltages (Fig. 4b). However, the increases in the voltage also raise the $CaCO_3$ formation energy from 16 kJ mol^{-1} CO_2 at 0.4 V to 188 kJ mol^{-1} CO_2 at 1.2 V (in full spectrum seawater) due to side reactions. The SO_4^{2-} ions have been demonstrated to negatively impact on the formation of $CaCO_3$(*25*), but the results showed the CDC technique can minimize the influence of SO_4^{2-} (Fig. 4b).

The CR is a critical parameter in ocean carbon removal techniques, as it influences the volume of seawater required to remove a specific amount of CO_2(*23*). A higher CR value can contribute to a reduction in the energy demands associated with seawater intake and pre-treatment stages. The maximal CR of 13% has been achieved in this work (Fig. 4c), which is still relatively lower than the CR of approximately 79% that has been reported

for the electrochemical pH swing method. Consequently, a large portion of the inorganic carbon remains unutilized. The electrochemical pH swing method, however, is independent on the inorganic carbon concentration levels. A promising research direction could be to develop a coupled system to treat seawater, which could enhance the utilization of inorganic carbons and improve the overall process efficiency.

We developed a 2D multiphysics model to delve into the $CaCO_3$ nucleation process, with the boundary conditions for ion concentrations setting to match experimental conditions (See Supplementary Note 3). The left boundary condition features Ca^{2+} ion concentrations ranging from 18 to 350 µmol (Fig. 4d). With a flow rate of 3ml min^{-1} (average velocity of 0.5 cm s^{-1}), and the average residence time—a measure of how long a fluid parcel remains in the channel—is 10 seconds (Fig. S16). Precipitation occurs if the nucleation induction time ($t_{induction}$) is less than the residence time ($t_{residence}$). Simulation results show that at a flow rate of 3ml min^{-1}, the maximum supersaturation (S) for an absorbed Ca^{2+} amount of 18 µmol is 26.0, which corresponds to a nucleation induction time of 77 seconds—significantly exceeding the residence time(*26*). Fig. 4e illustrates the minimum $t_{induction}$ across various experimental setups (Fig. S16, S17). The dashed line represents the $t_{residence}$, and the points below this line indicates conditions favorable for precipitation.

The CDC reactor was tested five consecutive cycles to treat fresh seawater without any cleaning procedures, and the consistent mass and energy consumptions of $CaCO_3$ produced suggests high reusability of the reactor (Fig. 4f). The morphology of the formed $CaCO_3$ was investigated using scanning electron microscopy (SEM), revealing a needle-like shape characteristic of aragonite (Fig. 4g), and this finding was further confirmed by X-ray diffraction

(XRD) analysis (Fig. 4h). No crystal structure conversion or dissolution of the aragonite was observed after three months in seawater (ambinet temperature and pressure), which demonstrates the high stability of the formed aragonite serving as an effective carbon storage medium in the epipelagic zone (Fig. 4h).

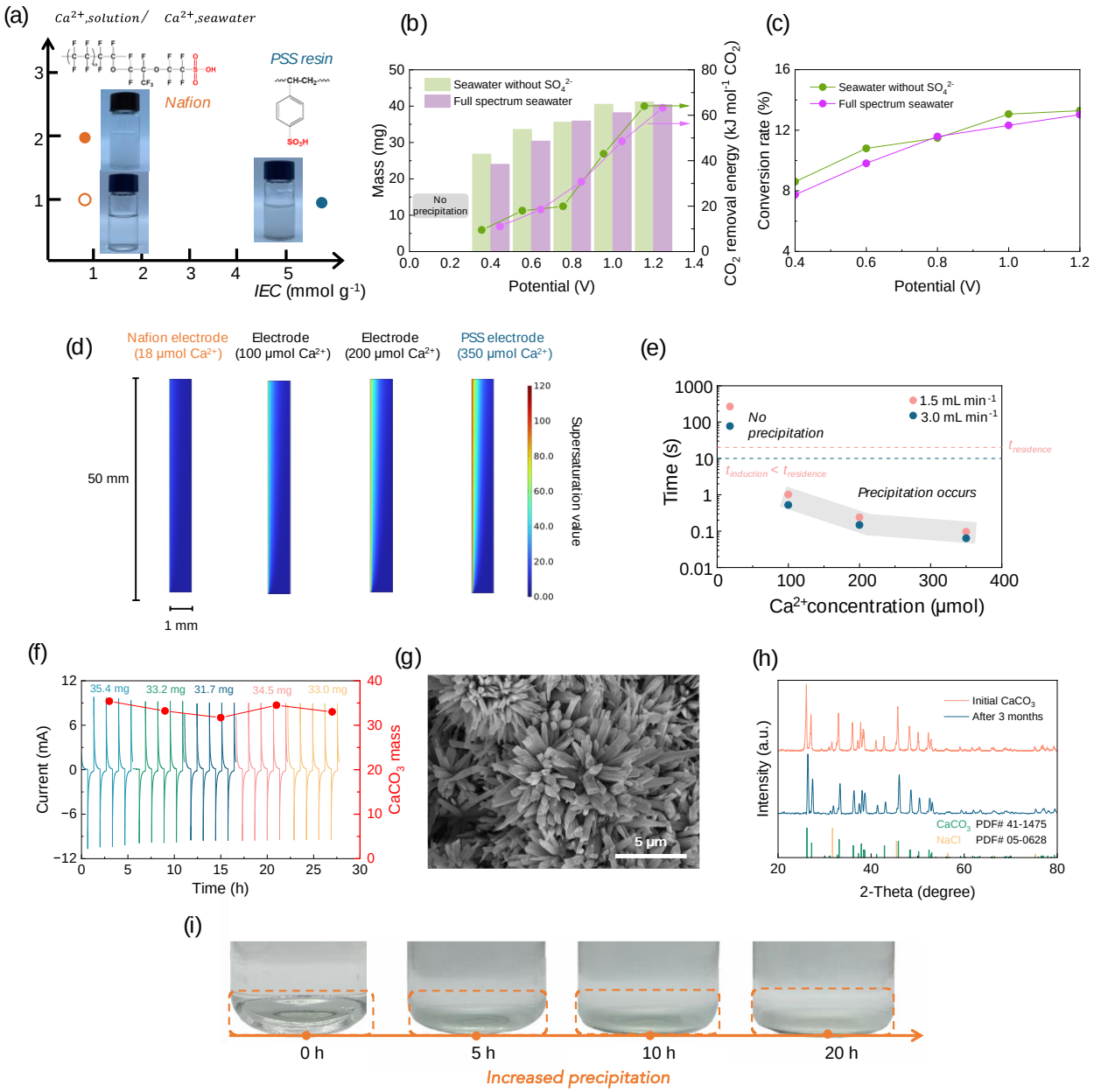

Fig. 4. $CaCO_3$ formation in a CDC reactor. (a) The experimetal observation of $CaCO_3$ formation when electrodes are decorated with polymers that possess varying ion-exchange capacities (IEC). $CaCO_3$ forms on the **Nafion electrode** at a concentration twice that of the Ca^{2+} present in seawater (solid dot), while on the **PSS electrode**, it forms at the concentration of seawater Ca^{2+}. (b) Relationship of the applied voltages and the mass of $CaCO_3$ produced and the energy consumptions. (c) Relationship between the applied voltages and CR values. (d) The supersaturation profiles under different bound Ca^{2+} concentrations of 18 to 350 μmol. The **Nafion electrode** and **PSS electrode** are able to bind with ~18 and 350 μmol based on the mass of polymer loaded on the electrode, and

the flow rate is 3.0 ml min^{-1}. (e) The induction times (dots) and residence time (lines) at the flow rates of 1.5 and 3.0 ml min^{-1}. (f) The current profile of a CDC reactor treating fresh seawater without any treatment for five consecutive cycles. (g) SEM image of $CaCO_3$. (h) XRD patterns of $CaCO_3$ upon initial formation and after three months. (i) The photos showing the mass of $CaCO_3$ at the bottom of the container gradually increases with time, up to 20 hours.

Energy and cost

The energy requirements for the ocean carbon removal are predominantly composed of three key steps: seawater intake, pre-treatment, and the CDC process (Fig. 5a, Supplementary Note 4)(*23*). We have evaluated the energy implications across three operational scenarios: stand-alone, floating, and a setup co-located with a desalination plant (i.e., co-located system) (Fig. 5b). Specifically, in the stand-alone scenario, seawater must be pumped into the facility and subjected to a multi-step filtration process prior to the CDC process(*24*). However, the CRC reactor is designed to be floated on the ocean surface, and the energy consumption associated with the seawater intake can be significantly reduced under the floating mode. The third scenario involves the facility being co-located with a desalination facility, enabling the absorption of seawater intake and pre-treatment energy by the existing infrastructure (Fig. 5b).

In the stand-alone mode, the total energy consumption amounts to 443.0 kJ mol^{-1} CO_2, with approximately 85% allocated to the process of seawater intake (Tab. S2). Nonetheless, this consumption can be significantly reduced when employing a floating mode. The energy consumption for filtration is at 53.5 kJ mol^{-1} CO_2, which is considerably higher than that for the CDC process (16.4 kJ mol^{-1} CO_2). An ideal approach to further improve the energy efficiency of the CDC involves integrating the CDC reactor with existing desalination facilities (Tab. S2), but it is limited by the global scale of desalination industries.

A techno-economic analysis (TEA) of CDC system was conducted to evaluate the feasibility of the proof-of-concept system using methods available in literature (Fig. 5a, See Supplementary Note 5). The plant scale was set to be 500,000 tonnes of CO_2 captured per year, with the inclusion of CDC reactor, solar energy, and battery storage systems (see details in the Supplementary Information)(*27*). The corresponding carbon capture costs for the stand-alone, floating, and co-located systems are \$467, \$151, and \$80 t^{-1} CO_2, respectively (Tab. S3). The produced $CaCO_3$ can be sold and utilized in various industries such as constructions, agriculture and medical applications to subsidize carbon removal costs(*28*), however, this profit was not counted considering the costs associated with the $CaCO_3$ collection and transportation are out of scope for this study.

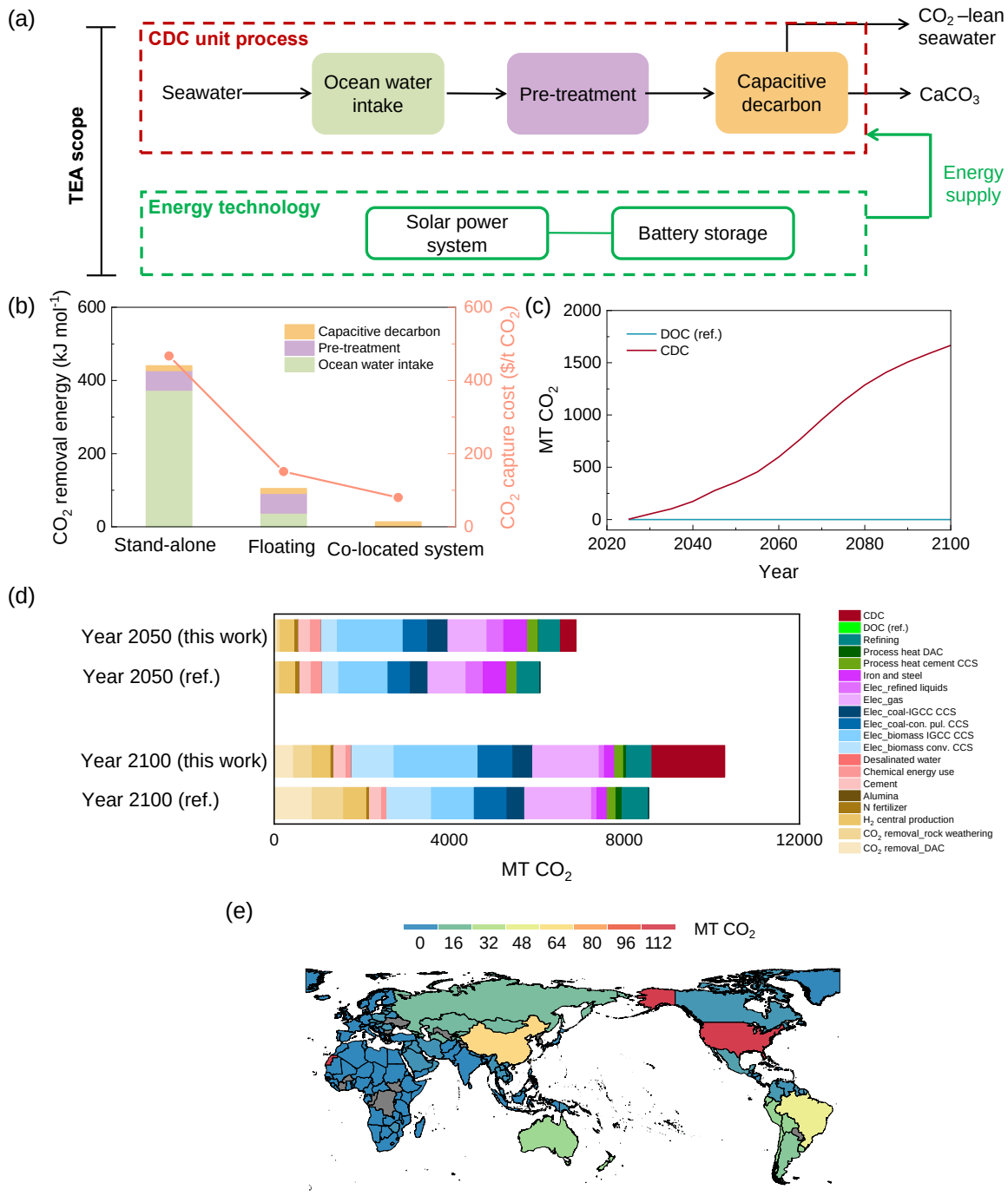

Fig. 5. Evaulation of the CDC technique. (a) The TEA scope of this work; (b) Energy consumption and CO_2 removal costs by the CDC technology under the scenarios of stand-alone, floating and the co-located system. (c) The simulated contribution of CDC and DAC to global carbon removal in the time span of 2025-2100 (Mt per year). (d) Global carbon sequestration profiles with a diverse techniques in year 2050 and 2100 simulated by GCAM. DOC is invisible in the reference bar graphs (e) Global carbon sequestration potentials by the CDC method and GCAM 32 regions in 2050.

Global Change Analysis Model (GCAM) for carbon sequestration analysis

An extensive range of carbon sequestration methods, including bioenergy with carbon capture and storage (BECCS), afforestation (AF), direct air capture with carbon storage, enhanced weathering, soil carbon sequestration, and direct ocean capture with carbon storage, has been rigorously investigated through TEA, biogeochemical, and ecosystem modeling(*8*). A recent study has incorporated the outcomes of these analyses into the Global Change Analysis Model (GCAM), an integrated assessment model characterized by its detailed technological specifications and its ability to provide an in-depth understanding of the interplay among diverse techniques and global carbon mitigation efforts (*1*).

We have modified the cost and performance parameters in GCAM to reflect the CDC technique, and then use the model to evaluate the impact of CDC on a global scale (Tab. S4, S5). Specifically, we referenced the floating scenario as the test condition, which is characterized by an energy consumption rate of 107 kJ mol^{-1} CO_2 and a removal cost of \$151 t^{-1} CO_2. We have chosen not to incorporate more aggressive operational modes, such as the co-located systems in this section, primarily on the consideration that the scale of desalination is limited and may not be commensurate with the gigatonne (Gt) scale of CO_2 removal demands.

The previously reported DOC technique, with its high energy inputs of 727 kJ mol^{-1} CO_2 and a substantial cost (non fuel) of \$1,700 t^{-1} CO_2, has faced significant limitations in scaling up (Fig. 5c).(*8*) Projections indicate that through the reported DOC method, only 0.0043 and 0.0085 million tonnes of CO_2 could be removed in the years 2050 and 2100, respectively (Tab. S5). However, with the introduction of the CDC process, there has been a remarkable enhancement in performance. The simulated results project that the CDC

process could remove up to 357 and 1,666 million tonnes of CO_2 in the years 2050 and 2100, respectively, indicating its capacity to contribute to climate change mitigation strategies on a global scale (Fig. 5c, d).

Our simulation results indicate that the contribution of the reference DOC technique to global carbon sequestration is negligible (<<1%). In contrast, the CDC process shows a substantially higher scale up potential. According to our simulations, the CDC technique could account for 4.55% and 14.82% of the global carbon sequestration in the years 2050 and 2100, respectively (Fig. 5c, d). These percentages suggest a significant increase in the contribution to global carbon mitigation efforts compared to the current DOC technique. America and China have the greatest potential for carbon sequestration by employing the proposed CDC technologies, potentially eliminating 109 and 68 million tonnes of CO_2 per year, respectively in 2050 (Fig. 5e). This advancement could play a crucial role in addressing climate change by providing a more effective means of reducing anthropogenic CO_2 levels.

Conclusion

In this work, we introduced an electrochemical technique for direct carbon capture from the ocean, converting it into $CaCO_3$. This method is chemical reaction-free and has a minimal environmental footprint, setting a new benchmark for low energy usage and a safe way to permanently sequester oceanic carbon. The appoarch lies in the use of a Ca^{2+} ion selective electrode that enriches Ca^{2+} ions from seawater, which then react with carbonate ions to precipitate $CaCO_3$. Through careful optimization of the electrode and reactor, we have achieved ocean carbon removal with remarkably low energy consumption, ranging

from 16 to 107 kJ mol^{-1} CO_2. Our TEA indicates that the cost of carbon removal could be less than \$150 t^{-1} CO_2 removed. As a proof-of-concept analysis, we employed the GCAM to assess the global impact of this approach and found that it could remove between 357 and 1666 million tonnes of CO_2 in 2050 and 2100, respectively, equating to 4.55% and 14.82% of the global carbon sequestration capacity for those years. Our results present a promising pathway for using electrochemistry to store ocean carbon at a low cost and with minimal environmental impact.

Author contributions

Z.B.Z and H.Z. supervised the project. Z.B.Z and K.Z. conceived the study and designed experiments. Y.Z. performed the experiments, M.L performed the Multiphysics modeling, J.F., Y.O. performed the GCAM analysis; Z.B.Z, H.Z., K.Z., Y.Z., performed the electrochemical and TEA analysis, made figures and drafted the initial manuscript. All authors contributed to the final manuscript writing.

Prof. Kuichang Zuo, ORCID: https://orcid.org/0000-0002-3922-8702;

Prof. Zishuai Bill Zhang, ORCID: https://orcid.org/0000-0002-9268-4889

Conflicts of interest

The authors (Z.B.Z, K.Z., and Y.Z.) have filed a patent related to this work.

Acknowledgements

This work was supported by the National Science Fund for Distinguished Young Scholars (Grant No. 21925801), and Peking University start-up funding.

Data availability

Data that support the findings of this study are presented in the main article and Supplementary Information files, or from the corresponding author upon request. GCAM is an open-source community model available at https://github.com/JGCRI/gcam-core/releases. The particular version of GCAM, additional input files and data-processing scripts associated with this study are available at https://doi.org/10.5281/zenodo.7492895.

1. J. Fuhrman, C. Bergero, M. Weber, S. Monteith, F. M. Wang, A. F. Clarens, S. C. Doney, W. Shobe, H. McJeon, Diverse carbon dioxide removal approaches could reduce impacts on the energy–water–land system. *Nat. Clim. Chang.* **13**, 341–350 (2023).

2. D. W. Keith, G. Holmes, D. St. Angelo, K. Heidel, A process for capturing CO2 from the atmosphere. *Joule* **2**, 1635 (2018).

3. E. S. Sanz-Pérez, C. R. Murdock, S. A. Didas, C. W. Jones, Direct capture of CO2 from ambient air. *Chem. Rev.* **116**, 11840–11876 (2016).

4. P. Zhu, Z.-Y. Wu, A. Elgazzar, C. Dong, T.-U. Wi, F.-Y. Chen, Y. Xia, Y. Feng, M. Shakouri, J. Y. Kim, Z. Fang, T. A. Hatton, H. Wang, Continuous carbon capture in an electrochemical solid-electrolyte reactor. *Nature* **618**, 959–966 (2023).

5. H. Li, M. E. Zick, T. Trisukhon, M. Signorile, X. Liu, H. Eastmond, S. Sharma, T. L. Spreng, J. Taylor, J. W. Gittins, C. Farrow, S. A. Lim, V. Crocellà, P. J. Milner, A. C. Forse, Capturing carbon dioxide from air with charged-sorbents. *Nature*, doi: 10.1038/s41586-024-07449-2 (2024).

6. S. Fahr, J. Powell, A. Favero, A. J. Giarrusso, R. P. Lively, M. J. Realff, Assessing the physical potential capacity of direct air capture with integrated supply of low-carbon energy sources. *Greenh. Gases Sci. Technol.* **12**, 170–188 (2022).

7. J. Young, N. McQueen, C. Charalambous, S. Foteinis, O. Hawrot, M. Ojeda, H. Pilorgé, J. Andresen, P. Psarras, P. Renforth, S. Garcia, M. van der Spek, The cost of direct air capture and storage can be reduced via strategic deployment but is unlikely to fall below stated cost targets. *One Earth* **6**, 899–917 (2023).

8. I. A. Digdaya, I. Sullivan, M. Lin, L. Han, W.-H. Cheng, H. A. Atwater, C. Xiang, A direct coupled electrochemical system for capture and conversion of CO2 from oceanwater. *Nat. Commun.* **11**, 4412 (2020).

9. C. Hepburn, E. Adlen, J. Beddington, E. A. Carter, S. Fuss, N. Mac Dowell, J. C. Minx, P. Smith, C. K. Williams, The technological and economic prospects for CO2 utilization and removal. *Nature* **575**, 87–97 (2019).

10. S. Kim, M. P. Nitzsche, S. B. Rufer, J. R. Lake, K. K. Varanasi, T. A. Hatton, Asymmetric chloride-mediated electrochemical process for CO_2 removal from oceanwater. *Energy Environ. Sci.* **16**, 2030–2044 (2023).

11. H. Li, Z. Tang, X. Xing, D. Guo, L. Cui, X.-Z. Mao, Study of CO2 capture by seawater and its reinforcement. *Energy (Oxf.)* **164**, 1135–1144 (2018).

12. H. S. Kheshgi, Sequestering atmospheric carbon dioxide by increasing ocean alkalinity. *Energy (Oxf.)* **20**, 915–922 (1995).

13. Z. Zhang, E. W. Lees, F. Habibzadeh, D. A. Salvatore, S. Ren, G. L. Simpson, D. G. Wheeler, A. Liu, C. P. Berlinguette, Porous metal electrodes enable efficient electrolysis of carbon capture solutions. *Energy Environ. Sci.* **15**, 705–713 (2022).

14. E. W. Lees, M. Goldman, A. G. Fink, D. J. Dvorak, D. A. Salvatore, Z. Zhang, N. W. X. Loo, C. P. Berlinguette, Electrodes Designed for Converting Bicarbonate into CO. *ACS Energy Lett.* **5**, 2165–2173 (2020).

15. Z. Zhang, E. W. Lees, S. Ren, B. A. W. Mowbray, A. Huang, C. P. Berlinguette, Conversion of Reactive Carbon Solutions into CO at Low Voltage and High Carbon Efficiency. *ACS Cent Sci* **8**, 749–755 (2022).

16. S. Ren, D. Joulié, D. Salvatore, K. Torbensen, M. Wang, M. Robert, C. P. Berlinguette, Molecular electrocatalysts can mediate fast, selective CO2 reduction in a flow cell. *Science* **365**, 367–369 (2019).

17. F. P. García de Arquer, C.-T. Dinh, A. Ozden, J. Wicks, C. McCallum, A. R. Kirmani, D.-H. Nam, C. Gabardo, A. Seifitokaldani, X. Wang, Y. C. Li, F. Li, J. Edwards, L. J. Richter, S. J. Thorpe, D. Sinton, E. H. Sargent, CO_2 electrolysis to multicarbon products at activities greater than 1 A cm^{-2}. *Science* **367**, 661–666 (2020).

18. J. Li, A. Xu, F. Li, Z. Wang, C. Zou, C. M. Gabardo, Y. Wang, A. Ozden, Y. Xu, D.-H. Nam, Y. Lum, J. Wicks, B. Chen, Z. Wang, J. Chen, Y. Wen, T. Zhuang, M. Luo, X. Du, T.-K. Sham, B. Zhang, E. H. Sargent, D. Sinton, Enhanced multi-carbon alcohol electroproduction from CO via modulated hydrogen adsorption. *Nat. Commun.* **11** (2020).

19. P. De Luna, C. Hahn, D. Higgins, S. A. Jaffer, T. F. Jaramillo, E. H. Sargent, What would it take for renewably powered electrosynthesis to displace petrochemical processes? *Science* **364** (2019).

20. G. Gadikota, J. Matter, P. Kelemen, P. V. Brady, A.-H. A. Park, Elucidating the differences in the carbon mineralization behaviors of calcium and magnesium bearing alumino-silicates and magnesium silicates for CO2 storage. *Fuel (Lond.)* **277**, 117900 (2020).

21. V. Romanov, Y. Soong, C. Carney, G. E. Rush, B. Nielsen, W. O'Connor, Mineralization of carbon dioxide: A literature review. *ChemBioEng Rev.* **2**, 231–256 (2015).

22. J. Strefler, T. Amann, N. Bauer, E. Kriegler, J. Hartmann, Potential and costs of carbon dioxide removal by enhanced weathering of rocks. *Environ. Res. Lett.* **13**, 034010 (2018).

23. C. L. Ross, T. M. DeCarlo, M. T. McCulloch, Environmental and physiochemical controls on coral calcification along a latitudinal temperature gradient in Western Australia. *Glob. Chang. Biol.* **25**, 431–447 (2019).

24. T. Liu, J. Serrano, J. Elliott, X. Yang, W. Cathcart, Z. Wang, Z. He, G. Liu, Exceptional capacitive deionization rate and capacity by block copolymer-based porous carbon fibers. *Sci. Adv.* **6**, eaaz0906 (2020).

25. Y. Zhu, Z. Gao, B. Lee, Y.-S. Jun, Process-specific effects of sulfate on CaCO3 formation in environmentally relevant systems. *Environ. Sci. Technol.* **56**, 9063–9074 (2022).

26. S. K. Myasnikov, A. P. Chipryakova, N. N. Kulov, Kinetics, energy characteristics, and intensification of crystallization processes in chemical precipitation of hardness ions. *Theor. Found. Chem. Eng.* **47**, 505–523 (2013).

27. N. McQueen, M. J. Desmond, R. H. Socolow, P. Psarras, J. Wilcox, Natural gas vs. Electricity for solvent-based Direct Air Capture. *Front. Clim.* **2** (2021).

28. Z. Mu, K. Kong, K. Jiang, H. Dong, X. Xu, Z. Liu, R. Tang, Pressure-driven fusion of amorphous particles into integrated monoliths. *Science* **372**, 1466–1470 (2021).